Proposal title:

"Advanced direct biogas fuel processor for robust and cost-effective decentralised hydrogen production" BioRobur^{Plus}

Topic:	FCH-02-2-2016. Development of compact reformers for distributed bio-hydrogen production
Funding scheme:	Collaborative project
Start date of project:	1st January 2017
Duration:	42 months

Deliverable: A dynamic model to investigate the dynamic response of the system under different operating strategies

Organisation name of lead contractor for this deliverable:

ETHNIKO KENTRO EREVNAS KAI TECHNOLOGIKIS ANAPTYXIS (CPERI)

Authors: G. Pantoleontos, N. Vlachos, S. Lorentzou

Dissemination level: Public

Index

1.   Introduction

In the previous report the steady state simulation and optimization of biogas reforming in a coated monolith channel was conducted [1]. In the current report the dynamic profiles of the major dependent variables are presented. The generic dimensionless dynamic model along with the reaction rates of the autothermal reforming of biogas presented in [1] hold, while the analysis is enriched by time scheduling features.

Transient analysis of such processes is of paramount importance: first of all, during the cold start-up operation the reactor's material properties and heat inertia terms are accounted for, so that idle times and time scheduling features are assessed; secondly, although the hydrocarbons reforming (e.g. steam-methane reforming in catalytic packed bed reactors) presents fast transients in the "hot" start-up operation, when integrated into a larger plant which includes intrinsically dynamic processes, such as PSA, H_2 storage units or fuel cells, its transients become relevant and interrelated to the overall plant's dynamics [2]. Furthermore, the transient simulation might depict peaks, such as hot spots, which are not captured by steady-state simulation [3]. Finally and most importantly, the dynamic model can be further extended, so that control and dynamic optimization techniques can be readily applied in order to analyze temperature or composition disturbances [4-5].

2.   Dynamic analysis

Dynamic models and transient analysis in monoliths have been also presented in the past; e.g. 1-D analysis by Aslanjan et al. [6], who investigated the three-way catalytic converter for gasoline engine exhaust gas after treatment and 3-D analysis by Jahn et al. [7], who conducted a study involving the exothermic reaction of CO oxidation taking place on the catalyst surface. Relevant transient analysis regarding catalytic reforming reactors has been presented by Adams & Barton [3] for water-gas shift reactors, and Ghouse & Adams [8] for steam-methane reforming reactors. The authors simulated the reactors' start-up from a hot state: the authors initially filled the reactors with nitrogen at the temperature and pressure conditions, in which the reactions would take place; after steady-state conditions have been reached, the reactor is introduced with the feed mixture. Feed and temperature disturbances were applied, so that the "new steady-state" conditions are investigated (see also Hayes et al. [9-10], Psyllos & Philippopoulos [11], Chan et al. [12-13]).

Significant work regarding dynamic optimization and control of reforming systems has been presented by Baldea & Daoutidis [14], in a series of publications by Seepersad et al. [15-16], who applied control schemes for an integrated coal gasifier/steam methane reformer system, and in integrated methanol reforming and fuel cell systems by Ipsakis et al. [4-5]. The flow distributions on the light-off, warm-up performance and the temporal variation of the solid temperature of a monolithic catalytic converter [17] and a plane-channel, methane-fueled microreactor [18], were investigated through numerical simulation (see also Oh & Cavendish [19], Zygourakis [20], Wanker et al. [21]).

3.   Results and discussion

In the previous report [1], in the absence of specific information there are physico-chemical properties and features of the monolith structure taken from relevant literature references in order to present a generic channel-washcoat-strut modelling approach, so that some insight is gained by the specific simulation and optimization features that have been envisaged in the course of project. Even so, the results, trends and conclusions of the steady-state report are true for the data chosen and valid for any relevant autothermal mode of operation in the biogas-reforming case.

In this report the data for the washcoat-catalyst zone are updated according to correspondence and cooperation with the partner Johnson Matthey[1], while the heat inertia terms (not used under steady-state conditions for the simulation) – density and heat capacity – of the monolith supporting material (strut) were incorporated according to correspondence and cooperation with the partner Engicer[2] (Table 1). The mass and heat transfer coefficients which determine mass and heat transfer between the channel and the washcoat are multiplied with 1.5 to account for enhanced transport due to the "distorted" design of the (1 1 1) cube (see the analysis and justification presented in [1]). The optimization procedure has been conducted once again to account for the updated data, whose results are presented in Table 2. Relaxation of the equilibrium constraints is included (slightly

---

[1] Email correspondence with Sara Calo (Sara.Calo@matthey.com) [23.11.2018 & 28.11.2018]
[2] Based on Sandro Gianella's email (sandro@engicer.com) [24.04.2018]

exceeding 10% deviation from equilibrium for reaction r_3) for numerical reasons – no optimization run lead to lower deviation, an indication that this criterion is too tight for the updated data and the model. For the optimal results of Table 2 dynamic simulation is performed, whose results are presented and analysed in the following sections.

The schedule sequence of the start-up procedure is summarized in

Figure 1: each box represents a procedure in series with the subsequent ones, meaning that each box has to start and end before the next one proceeds (all but the first one, whose outlet stream can be directly fed to the monolith) – the dashed boxes denote a procedure that it is not simulated in the current study; the dashed arrows denote a choice of disturbance to be applied. First, it is assumed that the medium to heat the monolith has already been heated up to the required temperature (here: 1045.4 K), so that the cold start-up of the monolith proceeds immediately: the monolith remains at ambient conditions; it is heated up by air (already at the required temperature) in order to aid the monolith to reach the "reforming" conditions under steady-state (negligible temperature variation). Secondly, after the monolith/catalyst have been preheated, the feed mixture enters the monolith. The period of the activation of the catalyst has been suppressed, as it presents no computational interest (it only adds up as an overall idle time). Third, after the reformate gas has reached steady-state conditions, temperature or steam or oxygen flowrate are perturbed from steady state.

Table 1: Data used for the updated optimization and dynamic simulation of the autothermal reforming case.

Washcoat and catalyst	
Density of the washcoat material[1] (kg/m^3)	1400
Density of the catalyst[1] (kg/m^3)	1400
Heat capacity of the washcoat[*] [22] $Cp = A + B*t + C*t^2 + D*t^3 + E/t^2$ (J/mol*K) t = temperature [K/1000]	A=102.429 B=38.7498 C=-15.9109 D=2.628181 E=-3.007551
Porosity of the washcoat[1]	0.357
Monolith material (strut)	
Density[2] (kg/m^3)	2800
Heat capacity of the strut[**] [22] $Cp = A + B*t + C*t^2 + D*t^3 + E/t^2$ (J/mol*K) t = temperature [K/1000]	A=20.50009 B=63.3717 C=-49.54023 D=14.82801 E=-0.759969
Strut thickness[2] (m)	0.001
Monolith (whole design)	
Diameter of the monolith[2] (m)	0.26
Length of the channel/monolith[2] (m)	0.37
Porosity of the monolith[2] (whole design)	0.87

[*] Resembling that of α-Al_2O_3 [**] Resembling that of SiC

Table 2: Steady-state optimization of the autothermal biogas reforming in the channel-washcoat-wall system for the updated data

Max(F_{H2}) (moles/s)	δ (μm)	T_0 (K)	CH_4 final conversion	O_2 final conversion	Deviation from equilibrium, r_1	Deviation from equilibrium, r_2	Deviation from equilibrium, r_3
2.23x10^{-5}	46.2	1045.4	0.941955	0.999927	0.063	0.039	0.111

3.1 Cold start-up

During the cold start-up of a monolith catalytic structure, the solid material has to be heated up to the reforming temperature. In an adiabatic case, no external heating is provided to the reactor, and the heat-up of the reactor's solid material and catalyst has to be performed exclusively by a preheated inert gas entering at the desired temperature. In this case, the dynamics of the solid reactor is determined by the heat inertia terms of the solid materials (densities and heat capacities), as no other sink/source term (non-reactive case) exists in this mode of operation.
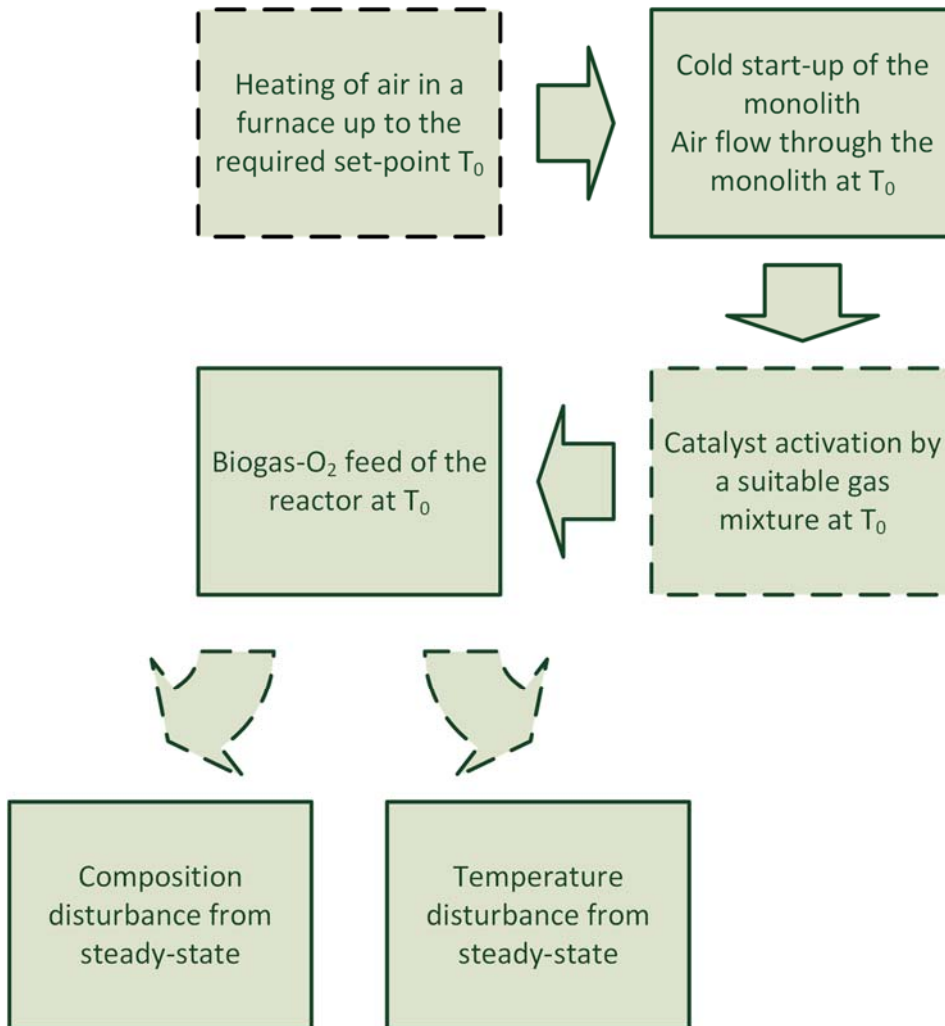
Figure 1: Schedule sequence of the start-up of the monolith.

Figure 2 depicts the contour plot of the axial monolith's wall temperature (SiSiC material) as a function of time when air enters the monolith at time t=0 and T_0=1045.4 K. As can be seen, the solid material's temperature initiates from ambient conditions (298 K) and needs a significant amount of time to reach the reforming temperature. During the cold start-up of the monolith it is evident that axial temperature is far from uniform: as the monolith is only heated by the flowing preheated air (as the heating medium) and not by, say, direct external radiation of a burner as in industrial reformers, the part of the wall close to the inlet is heated first, and the upper part follows. The overall monolith exceeds 977 K after 1.45 h of heating (red region covers the range 977-1045.4 K), and reaches the steady-state temperature after 4.35 h. It has to be noted that the computational steady-state deviation from 1045.4 K has been set to ≤0.1%.
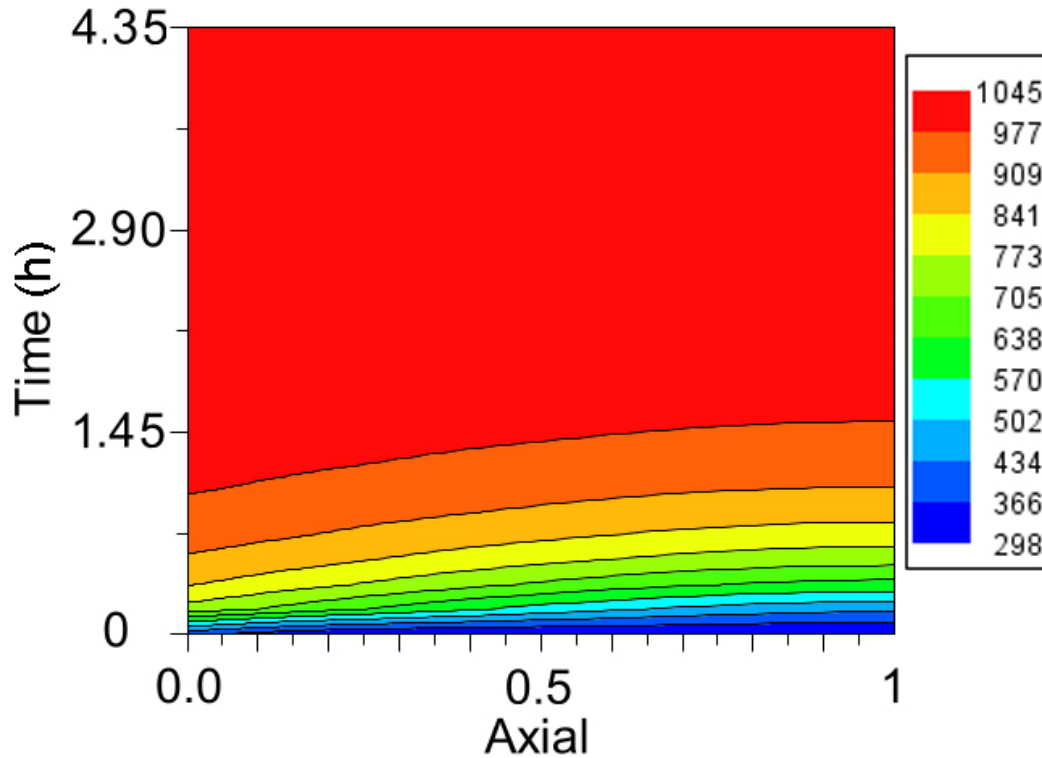
Figure 2: Contour plot of the solid outer wall temperature along $\hat{x}$ over time (cold start-up case).

Figure 3 shows the variation of axial temperature in the channel (averaged over y) and at the outer wall of the monolith-strut at various time instants. The flowing preheated gas (air) loses heat entering the monolith trying to cope with the huge heat demands of the solid material, which initiates from ambient temperature: during the first 26 s, only in the first part of the monolith, air (in the channel) and strut temperatures exceed 300 K. After 391 s the upper part ($\hat{x}$=1) of the strut's wall has already reached almost 400 K. Heating of the monolith proceeds fast in the first minutes because of the huge temperature gradients (flowing gas temperature versus almost ambient solid's temperature), but it then slows down: only after 45 min the upper wall's temperature has exceeded 850 K. After 180 min channel and wall temperature profiles are hardly distinguishable, but still not under steady-state conditions: at $\hat{x}$=0 they are T=1045.11 K, T_w=1041.54 K; at $\hat{x}$=1 they are T=1037.16 K, T_w=1037.15 K.

Figure 4 illustrates the dynamic variation of temperatures in the channel (averaged over y) at $\hat{x}$=0 and at the outer wall of the monolith-strut at $\hat{x}$=0 and at $\hat{x}$=1. After 26 s the heating medium temperature at $\hat{x}$=0 has dropped to 1006 K. Close to $\hat{x}$=0 the outer strut's wall reaches faster air's temperature and eloquently steady-state temperature (1045.4 K), rather than the upper point at $\hat{x}$=1 (cf. also Figure 3), which needs more time.

Figure 5 illustrates temperature snapshots with respect to $\hat{x}$ and $\hat{y}$ of the gas temperature in the channel zone. It is evident that there is also variation with respect to $\hat{y}$ especially in the first time periods, whereas $\hat{y}$-profiles flatten at later times and for $\hat{x}$≥0.1. Temperature gradients with respect to $\hat{x}$ exist for the whole heating period, and disappear for t=261 min (4.35 h), when the temperature difference of the upper $\hat{x}$-point ($\hat{x}$=1) and T_0 (=1045.4 K) has a deviation of ≤0.1%.
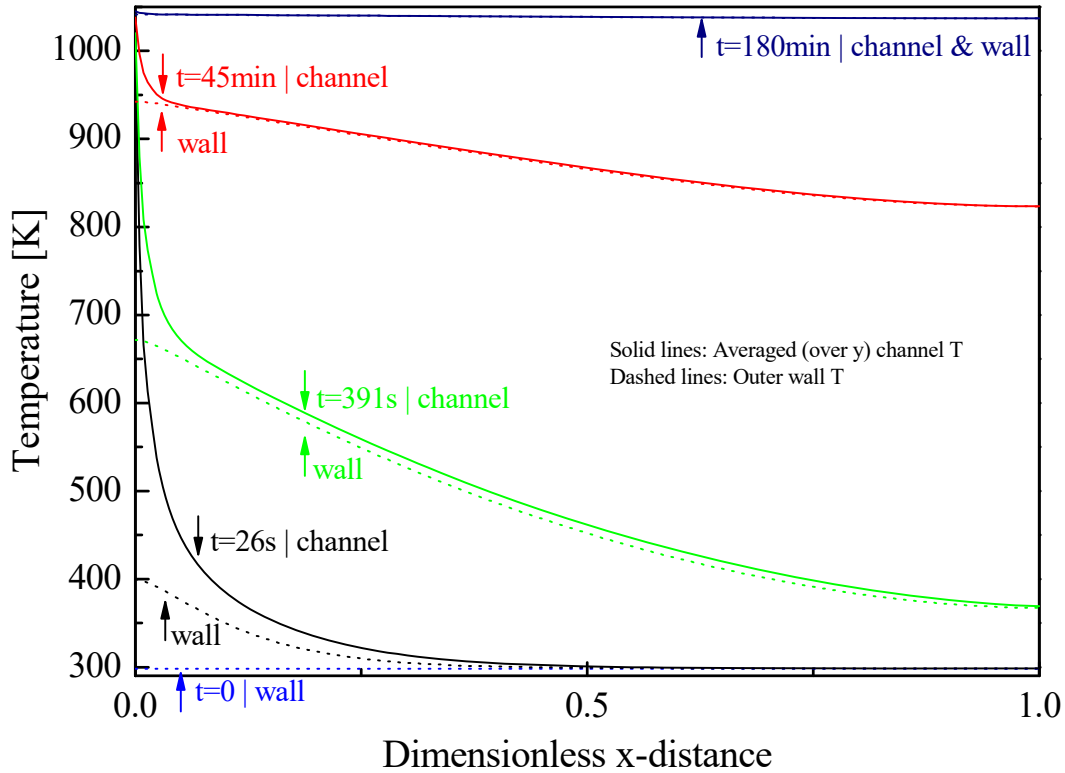
Figure 3: Transient temperature profiles during cold start-up operation. The solid lines are the gas temperature profiles in the channel zone (averaged over y) and the dashed lines are the solid temperatures at the outer wall ($\varphi_S=0$).
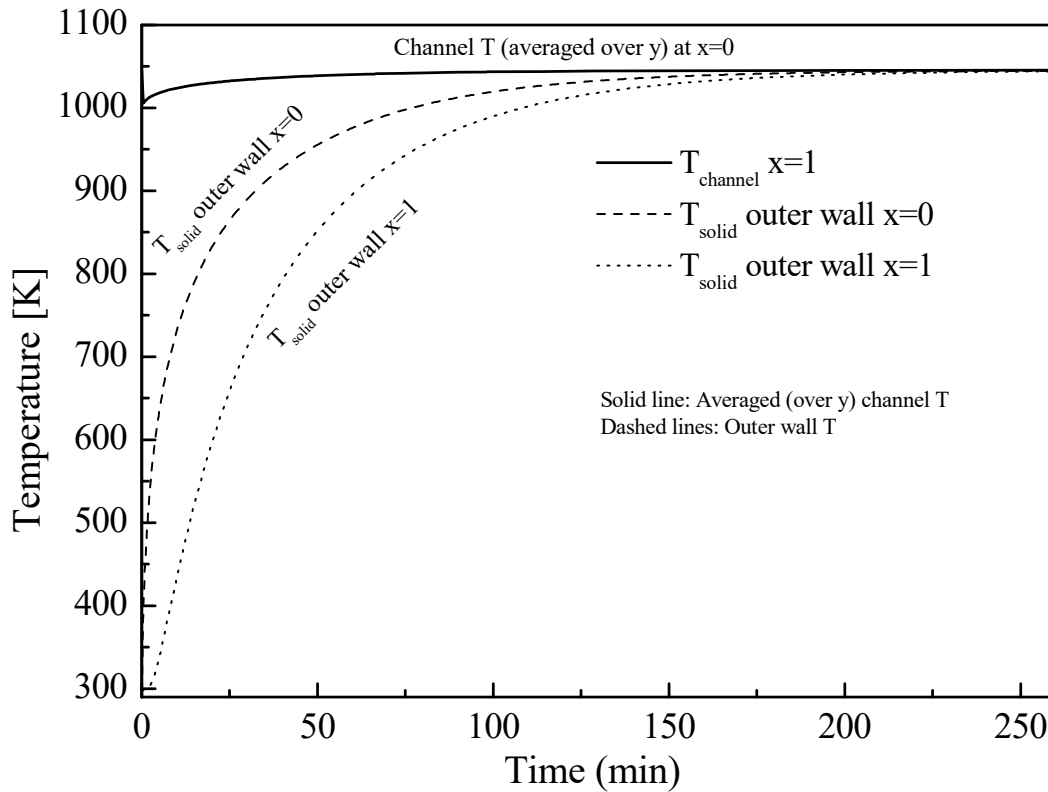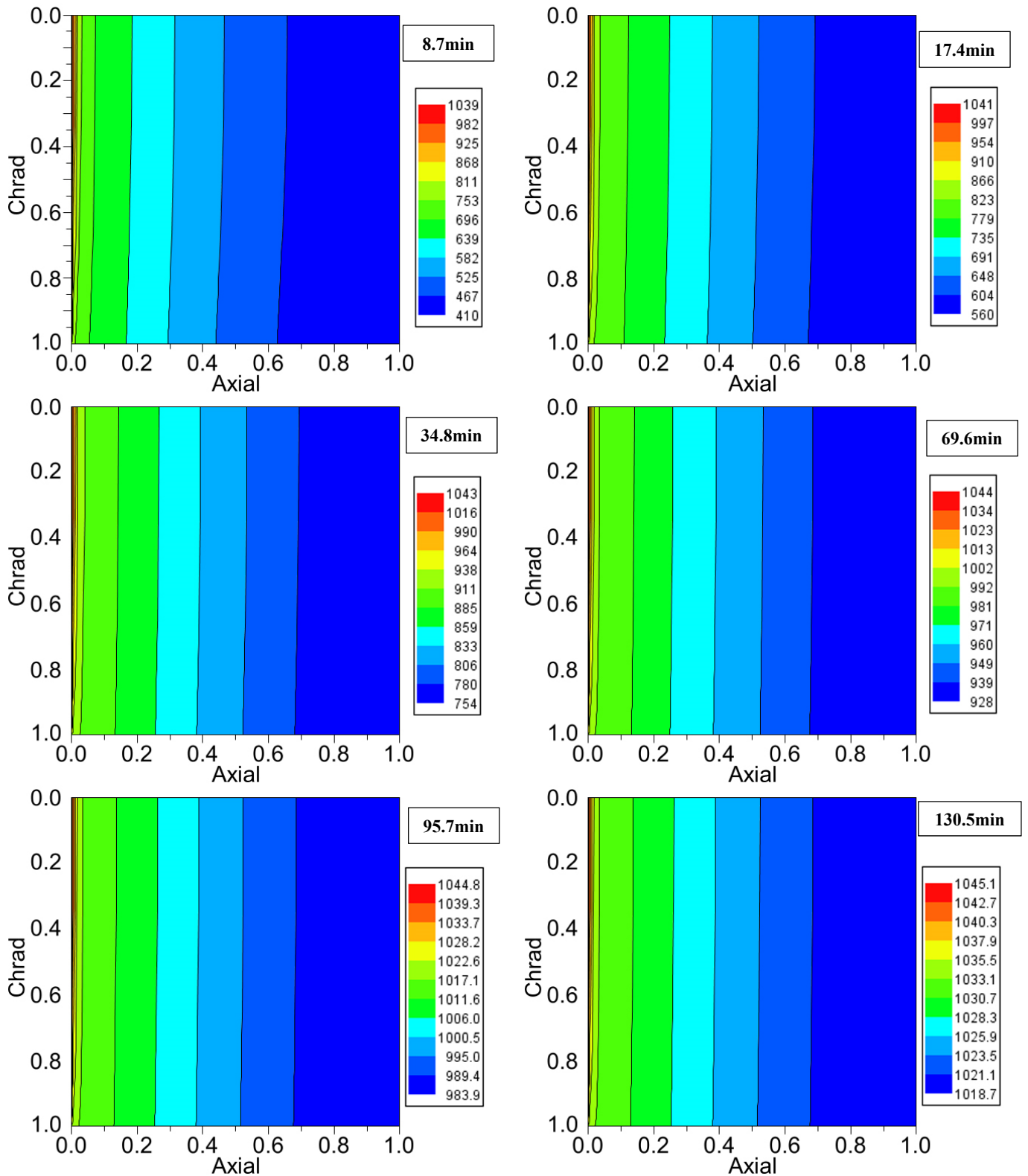

Figure 4: Transient temperature profiles of the gas in the channel zone (averaged over y) in the monolith's inlet and solid temperatures at the outer wall ($\varphi_S=0$) at two different x-points (cold start-up case).
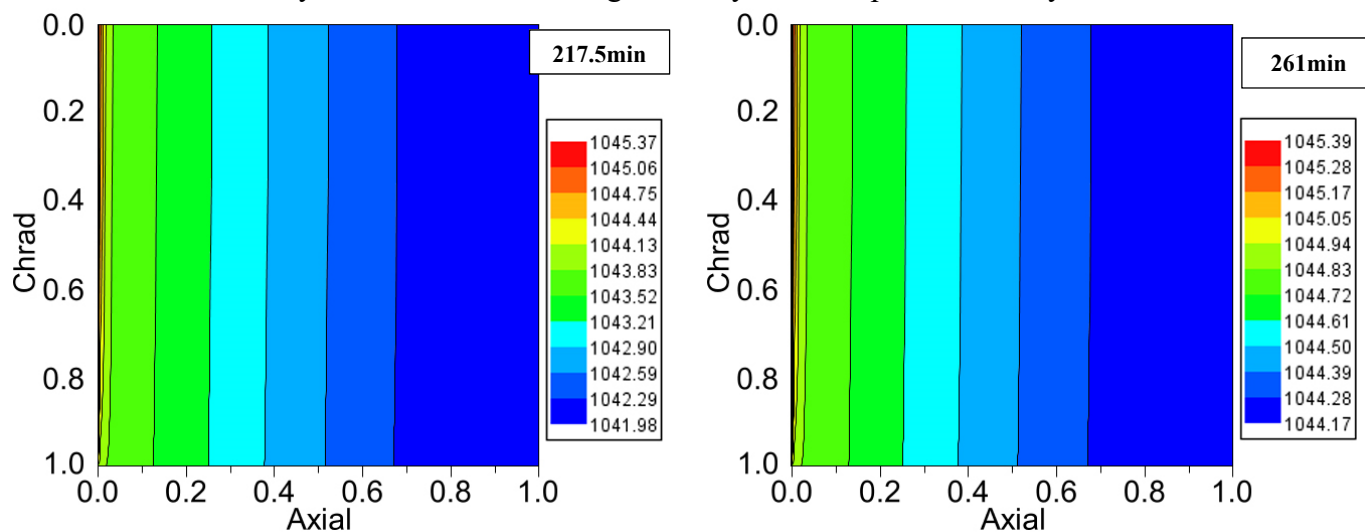
Figure 5: Contour plots of the gas temperature in the channel zone at different times (cold start-up case).

3.2 Biogas feed (reactive case)

When the monolith has reached the desired reforming temperature (t=4.35h and close to 1045.4 K, see comments above in section 3.1), the biogas mixture along with O_2 as defined in [1] enter the monolith reactor at 1045.4 K (sustaining a close-to-autothermal mode), that is, switching from an air mixture to the biogas-O_2 mixture at the same temperature T_0=1045.4. Due to the fact that solid materials are already at the required temperature, catalytic reactions at the washcoat initiate rather instantly, and methane conversion exceeds 94.196% under steady-state conditions, which are reached after 78 min (see Figure 6).
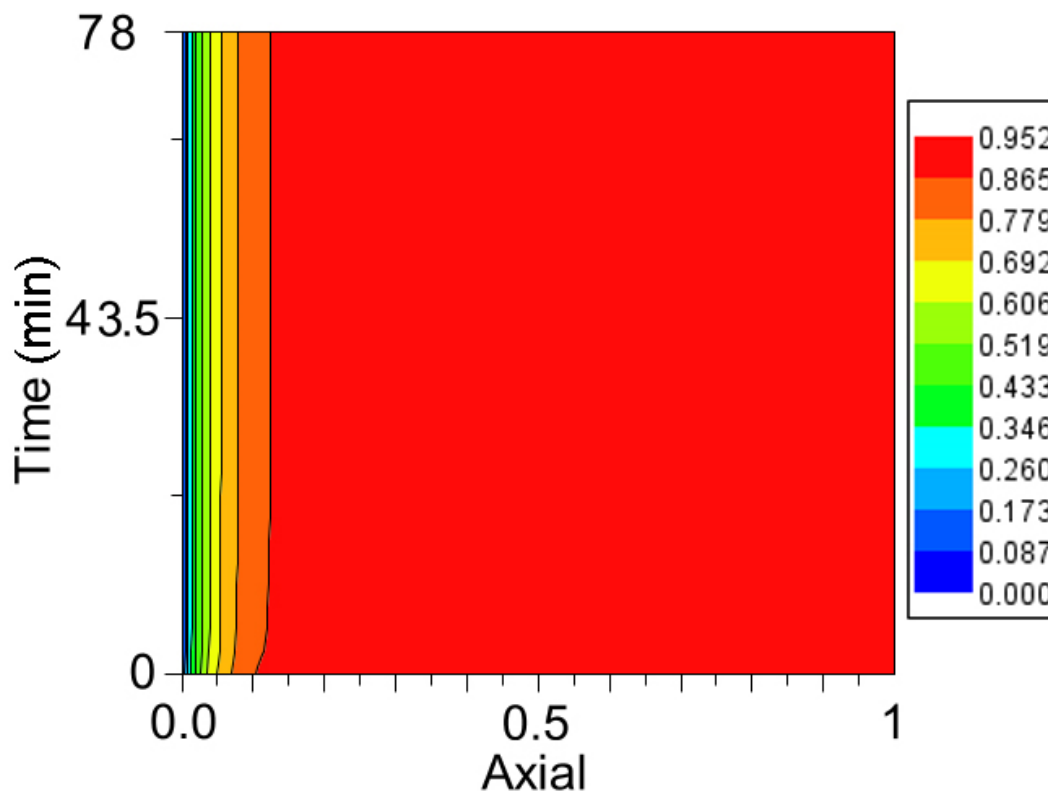

Figure 6: Contour plot of the CH₄ conversion in the channel along x over time.

Figure 7 depicts the molar fractions of the reformate gas from t=0 to 78 min at x=1. The flowrates do not get the steady-state values immediately, but it takes 78 min. The system response in a hot start-up case (starting from a preheated catalyst) is much faster than the cold start-up case because of the higher heat inertia terms in the latter case that have to be overpassed. As shown in the previous report [1] the diffusional limitations are very small, thus virtually resulting to no discrepancy between diffusion and reaction rates within the porous catalytic washcoat, which entails that products formation begins immediately taking advantage of the major part (along the depth) of the washcoat catalyst.

Nevertheless, there is a response delay along the x-distance during time evolution as the upper x-points get the new information (of the step change) later than the points closer to the inlet. For example, referring to Figure 8, the CH_4 molar fraction profile depicts a local minimum in the middle of the channel (x=0.5) after ~2.5 min from the transition to the reactive mode (t=0), which is propagated towards the exit (x=1) after 5 min (from t=0). Similar behavior can be found in the H_2O profiles. Of course, since both CH_4 and H_2O are reactants, they depict lower molar fractions at the channel's exit.
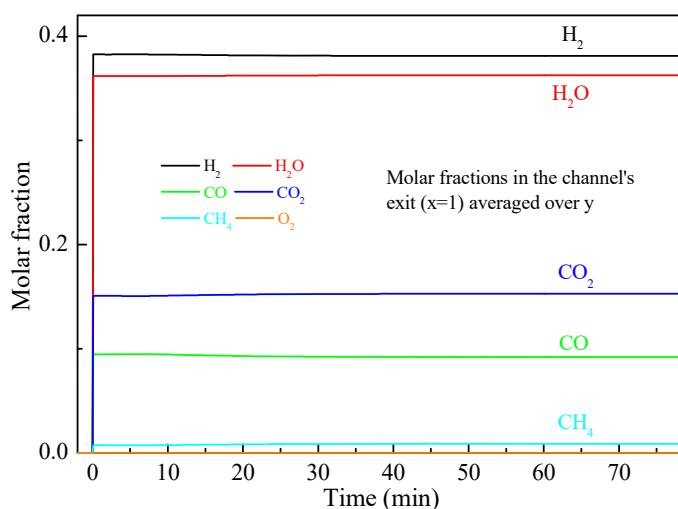

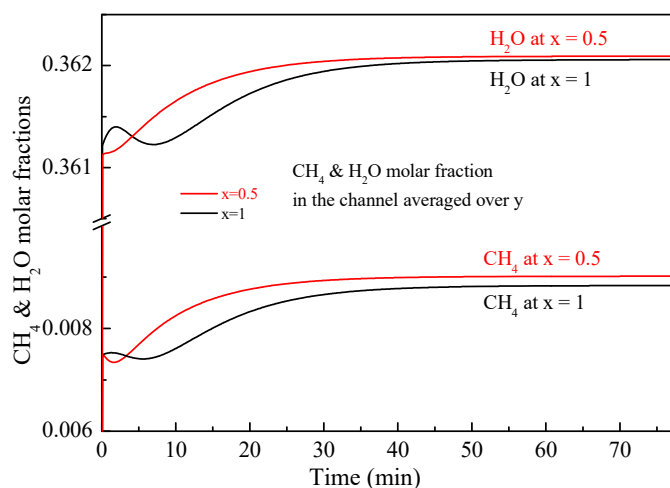**Figure 7: Transient molar fraction profiles in the channel zone (averaged over y) for the hot start-up case.**

Figure 8: Transient CH_4 and H_2O molar fraction profiles in the channel zone (averaged over y) at two x-points for the hot start-up case.

3.3 Temperature step and linear change

The third and final step of the dynamic simulation cases involves operation under disturbances, that is, after the reforming process has reached steady-state conditions using the data of Table 1 and the optimal results of Table 2 the system is perturbed from steady-state by introducing changes in the assigned values of e.g. T_0 and feed composition. Such a disturbance of a change in temperature could occur, e.g. in the case of a faulty or de-calibrated thermocouple in the preheater of the reactor [14], or a faulty mass flow controller, respectively.

The first disturbance from the (previous) steady state concerns the decrease of the feed temperature by 50 K. Two cases are considered; first, a step decrease (at t=0$^+$) of 50 K is imposed. This is an extreme case: practically, this may happen if there are two feed lines with the same molar flowrates and compositions, but at different temperatures. Suddenly, the feed line switches from the one at 1045.4 K to the other at 945.4 K. The second case assumes that the furnace heating the feed gas has been imposed a temperature ramp decrease of 15 K/min ending to 50 K decrease (that is, ending after 200 s having a value of 945.4 K).

In the latter case (temperature ramp) the temperature gradients are not so severe compared to the extreme step change. As seen in Figure 9, for the step-change case the least temperature after 21 s reaches 876 K very close to the inlet at the outer wall. As seen in Figure 10, for the temperature-ramp case the least temperature after 200 s reaches 882 K very close to the inlet at the outer wall. Thus, it can be concluded that for smaller temperature ramp values the temperature decrease in the wall, and consequently in the washcoat, is not so severe. This conclusion can be further supported by the temperature minimum values of Figure 11 and Figure 12, which

indicate that for the step-change case the minimum value is 870.6 K, while for the temperature-ramp case the minimum is 882.1 K. Both cases reach the new steady-state profile after 91.4 min.
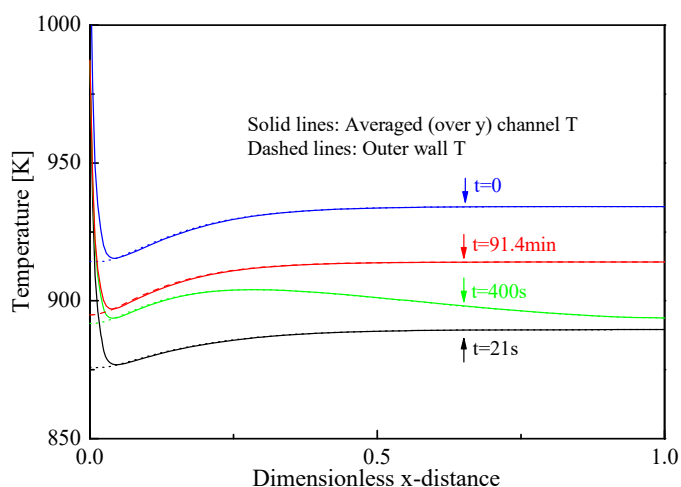

Figure 9: Transient temperature profiles for a step-change temperature decrease (t=0) from 1045.4 to 995.4 K. The solid lines are the gas temperature profiles in the channel zone (averaged over y) and the dashed lines are the solid temperatures at the outer wall (ϕ=0).

Figure 10: Transient temperature profiles for a temperature ramp of 15 K/min ending at t=200s from 1045.4 to 995.4 K. The solid lines are the gas temperature profiles in the channel zone (averaged over y) and the dashed lines are the solid temperatures at the outer wall (ϕ=0).
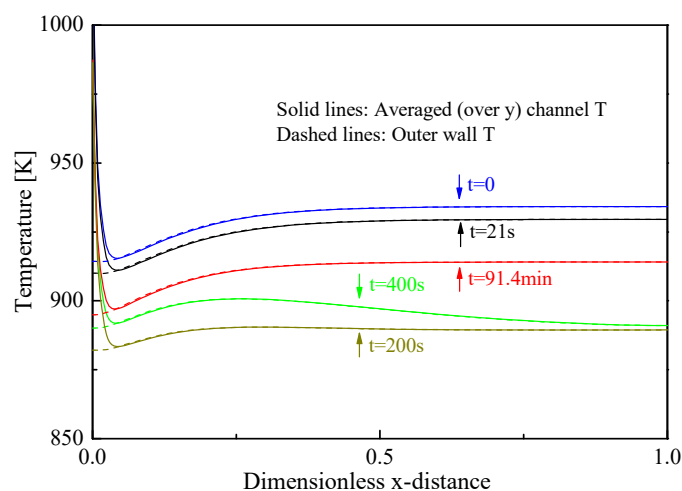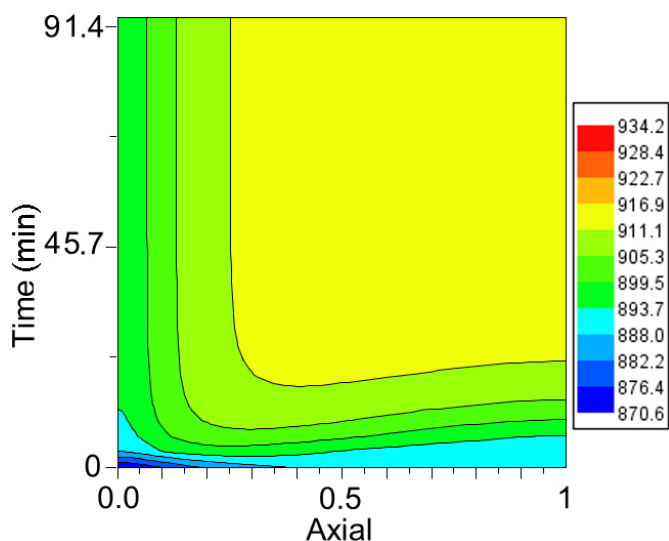

Figure 11: Contour plot of the solid outer wall temperature along x over time for a step-change temperature decrease (t=0) from 1045.4 to 995.4 K.

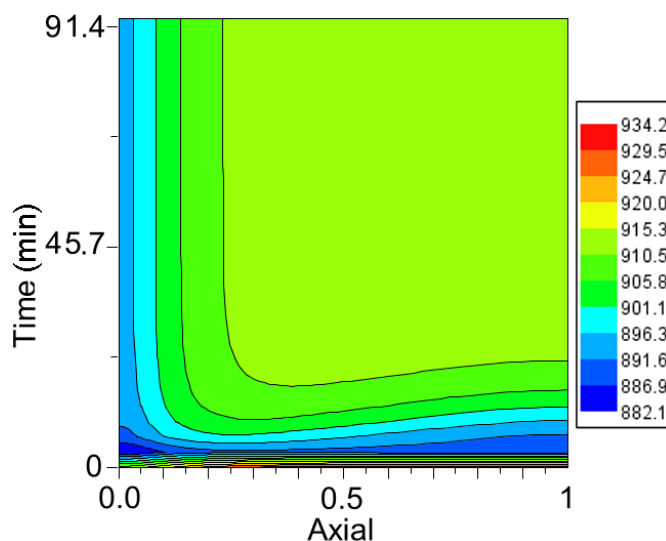**Figure 12: Contour plot of the solid outer wall temperature along x over time for a temperature ramp of 15 K/min ending at t=200s from 1045.4 to 995.4 K.**

The two cases with respect to methane conversion are drawn in the same figure, Figure 13. It is shown that for both cases there is a time lag for the profiles to get the information at the exit of the channel compared to the inlet (same colors – x=0 vs. x=1), since the profiles are steeper close to the inlet (after the new temperature has been imposed) and smoother near the exit. Comparing the two cases the temperature-ramp case is smoother than the step-change case because of the higher minimum temperatures in the former case (see also comments above regarding Figure 11 and Figure 12). Both cases exhibit the same final CH_4 conversion reaching 90.589 % after 91.4 min: the new steady-state conversion is significantly lower than that of the optimal case of [1] because of the decrease of the inlet temperature by 50 K.
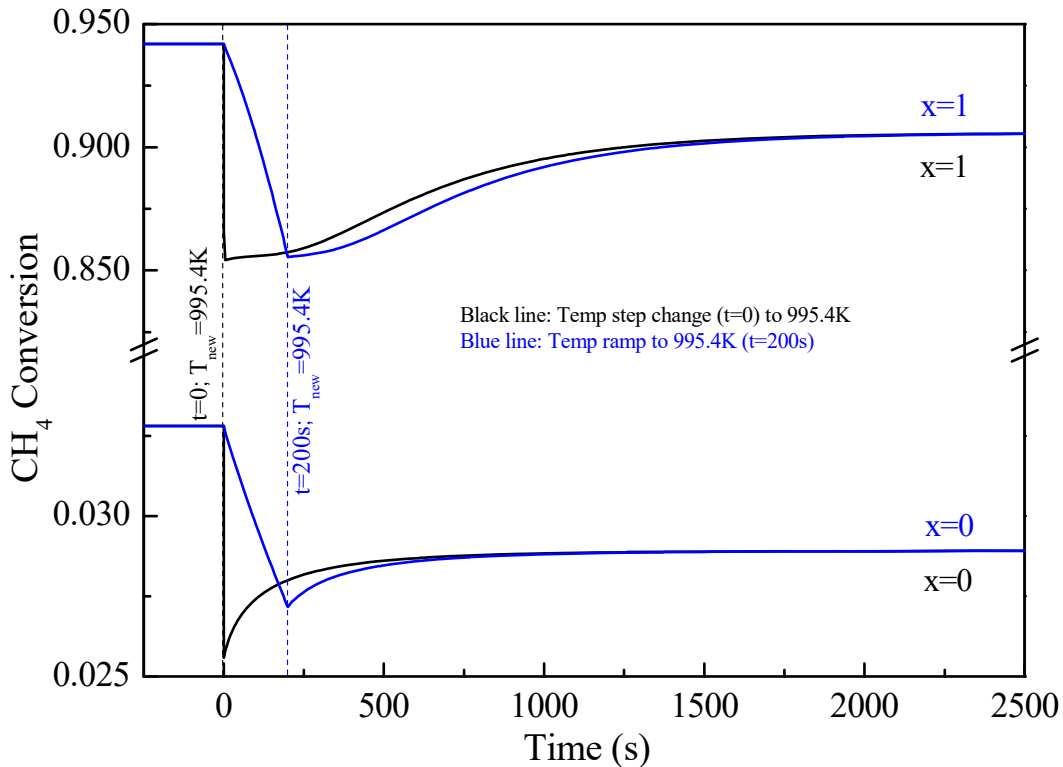
Figure 13: Transient CH$_4$ conversion profiles in the channel zone (averaged over y) for a temperature step change (t=0) and a temperature ramp (t=200s), from 1045.4 to 995.4K, at two different x-points (reactive case).

3.4 Oxygen step change

Suppose that the system has reached steady-state conditions in the hot start-up case after introducing the feed mixture according to the data of Table 1 and Table 2 (see section 3.2). Now, instead of temperature changes (see section 3.3) the composition of the biogas-O$_2$ mixture is altered. In this case, a step-decrease of the O$_2$ supply by 50% is imposed at t=0$^+$ (T$_0$ remains at 1045.4 K).

The inadequacy of the O$_2$ amount to sustain the autothermal mode is more pronounced in the O$_2$-decrease case leading to a drop of the final steady-state CH$_4$ conversion to 67.619 % after 90 min of operation, as illustrated in Figure 14. The double-axis graph in Figure 14 compares the dynamic evolution of the averaged (over y) CH$_4$ conversion and the averaged (over y) temperature at the channel's exit. For t<0 the steady-state values for the optimal reforming case (see section 3.2) at the exit are CH$_4$ conversion = 0.941955 and T=934.22 K; at t=0$^+$ a step-decrease of O$_2$ flowrate by 50% is imposed, which results to an almost immediate step-change of CH$_4$ conversion at the exit (the system is re-initialized by the software for the new assigned conditions). However, the temperature response does not follow the response of the conversion, but it has a delay; in this case the eventual temperature decrease to appear in a short course of time would be an indirect result of the smaller oxidation rate of CH$_4$, and not by any direct temperature decrease of the feed mixture as in the previous case (see section 3.3). After the first seconds of operation, temperature and conversion appear to have quite the same behavior.

The conversion decrease follows the decrease of the temperature in the catalytic washcoat since the decreased O$_2$ amount cannot maintain the endothermic reforming reactions needs. In Figure 15 a global temperature minimum equal to 838.1 K can be discerned close to x=0 under steady-state conditions, that is, a drop of 76 K (from the previous steady-state global minimum of 914 K). Still, this temperature drop does not entail that any carbon may be produced: even if no O$_2$ is present ("pure" biogas-steam reforming case) thermodynamic modelling analysis reveals that temperature has to drop below 500 K for potential carbon-forming conditions considering the composition of the biogas-steam as chosen in the course of the project (see [1]).
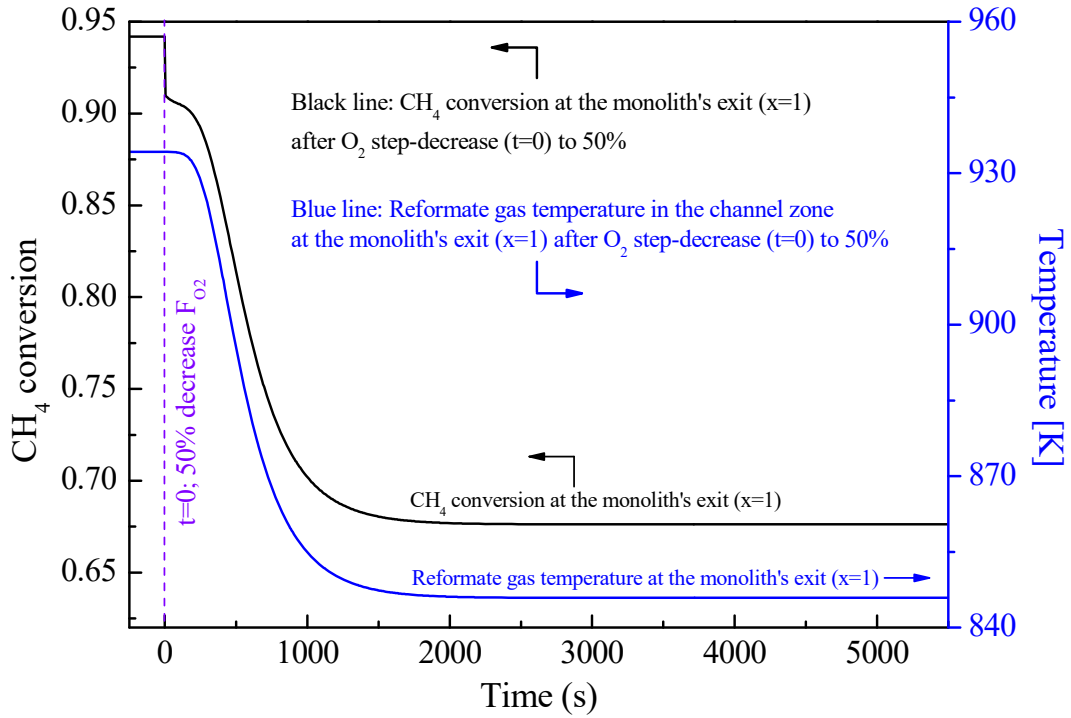
Figure 14: Transient CH₄ conversion and reformate gas temperature profiles in the channel zone (averaged over y) for a step-O₂ decrease (t=0) to 50%.
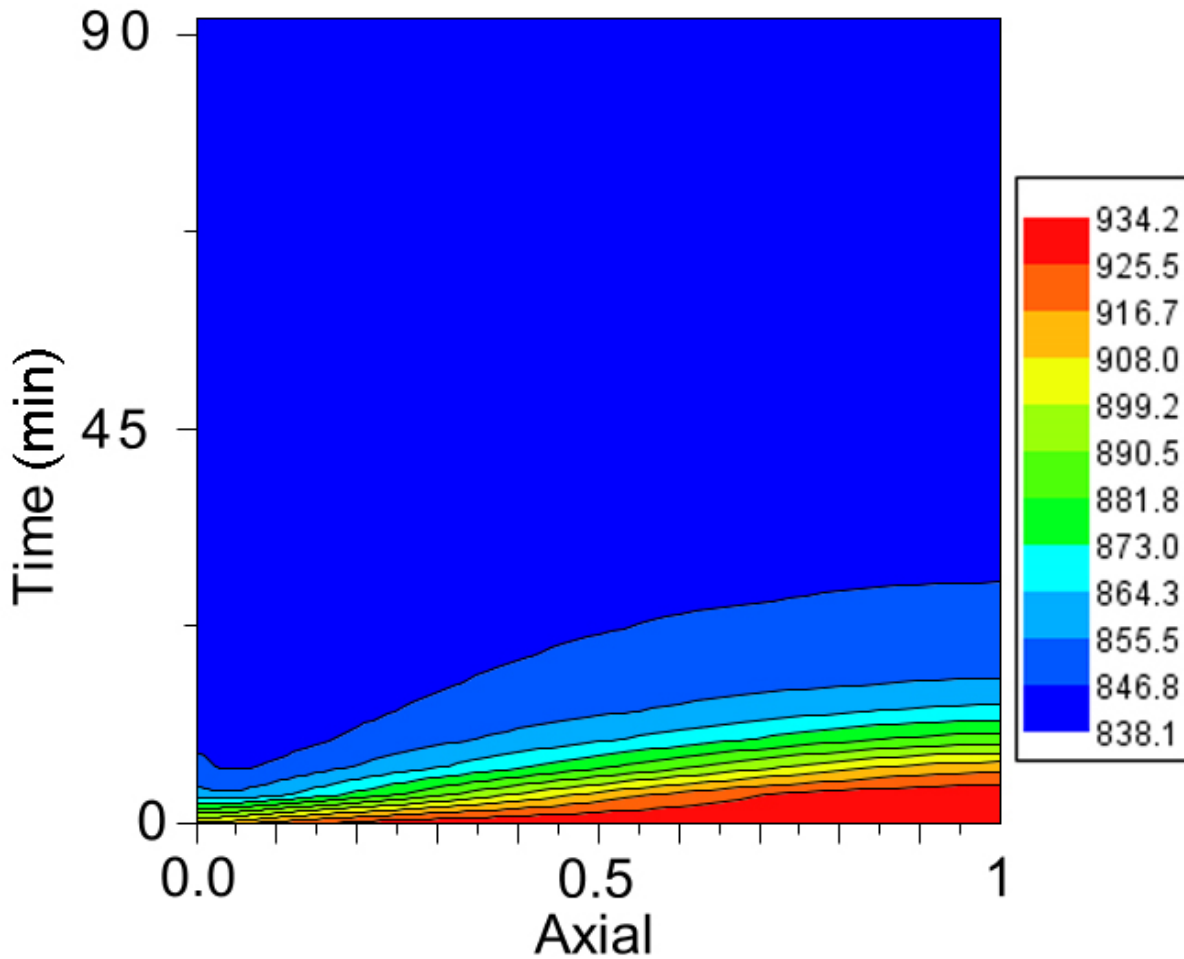

Figure 15: Transient temperature profiles at the washcoat-strut interface for a step-O₂ decrease (t=0) to 50%.

13

Figure 16 illustrates the response and the evolution of the flowrates at the channel's exit for the step O_2-decrease case for 50 s; this response – sudden increase or decrease of the flowrates – differs from the final value of the flowrates, e.g. H_2 flowrate suddenly increases, but it ends up with much smaller flowrate under steady-state conditions. In the following lines an interpretation of the flowrates' short-term response is attempted. In this analysis the general reaction scheme of four reactions (presented in [1]) is used.

Oxygen is considered to partake only in (R4) reaction, which involves consumption of CH_4 and formation of H_2O and CO_2. A sudden decrease of O_2 entering the reactor may lead to temporal increase of CH_4 and decrease of H_2O and CO_2. Nevertheless, in the long-term, the loss of O_2 leads to less heat generated by the CH_4-O_2 oxidation reaction, and eventually to the inability of facilitating the endothermic set of reforming reactions and to the drop of temperature, a fact that does not favour H_2 formation.
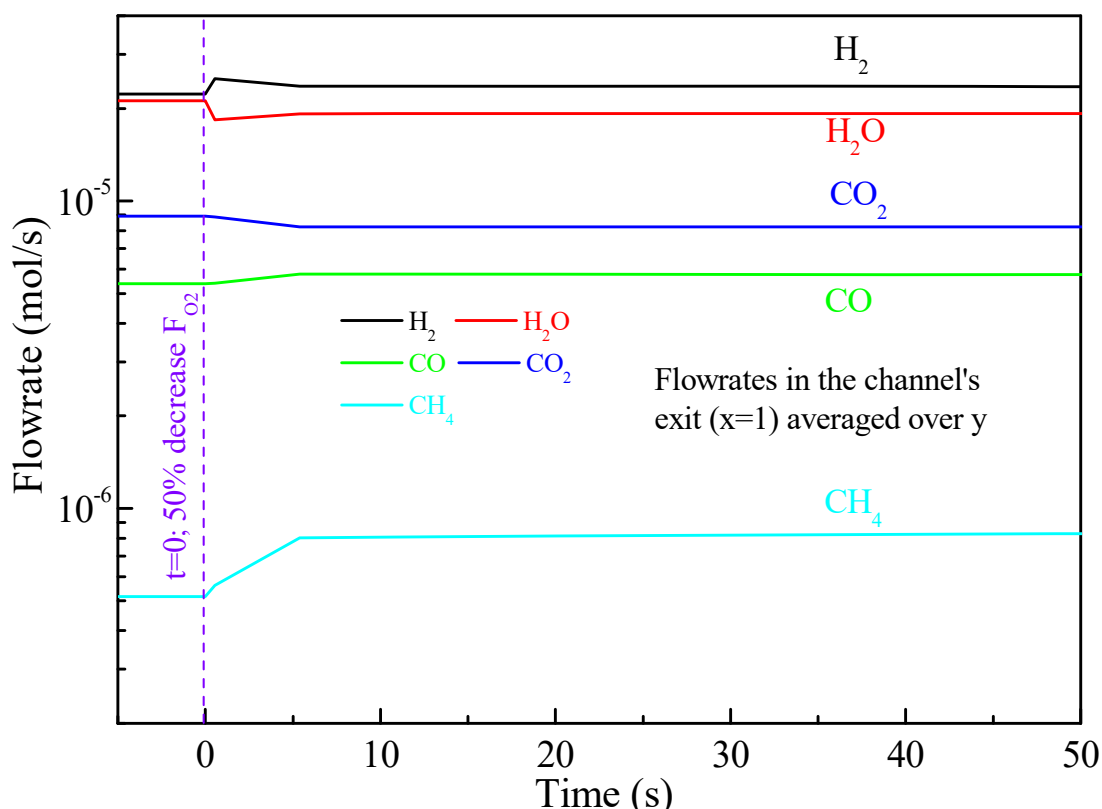

Figure 16: Transient molar fraction profiles in the channel zone (averaged over y) for a step-O_2 decrease (t=0) to 50% for the first 50s after the step-change.

3.5 Steam step change

Suppose that the system has reached steady-state conditions in the hot start-up case after introducing the feed mixture according to the data of Table 1 and Table 2 (see section 3.2). Now, instead of temperature changes (see section 3.3) or decrease of O_2 supply (see section 3.4), the composition of the steam is altered. In this case, a step-decrease of the H_2O supply by 45% is imposed at $t=0^+$ (T_0 remains at 1045.4 K).

The sudden drop of steam entering the monolith causes a step change in the CH_4 conversion (the system is re-initialized by the software for the new assigned conditions) at the channel's exit to less than 90%, a value that is roughly maintained during the autothermal reforming mode, ending to 87.627% after 90 min, as illustrated in Figure 17. The double-axis graph in Figure 17 compares the dynamic evolution of the averaged (over y) CH_4 conversion and the averaged (over y) temperature at the channel's exit. As can be seen, the temperature response does not follow the conversion's response, but it has a delay, as in the case of the oxygen-step change (see section 3.4). In the reactive mode of operation the reformate gas performs two tasks: first, by entering at 1045.4 K it crudely maintains the high temperature of the catalyst – since there is no other heating medium, such as an external burner like in the industrial reformers – and secondly, it produces carbon oxides and hydrogen in the catalytic washcoat. Since steam comprises the major fraction of the feed stream, its flowrate's sudden drop may cause a slight cooling of the solid material and subsequently of the gas temperature as well. Eventually, less steam in the

14

mixture does not favor the endothermic reforming reactions causing a slight increase of temperature: its value is somewhat higher than that of the original (optimal) case (936.2 K from 934.2 K – as illustrated in Figure 18).
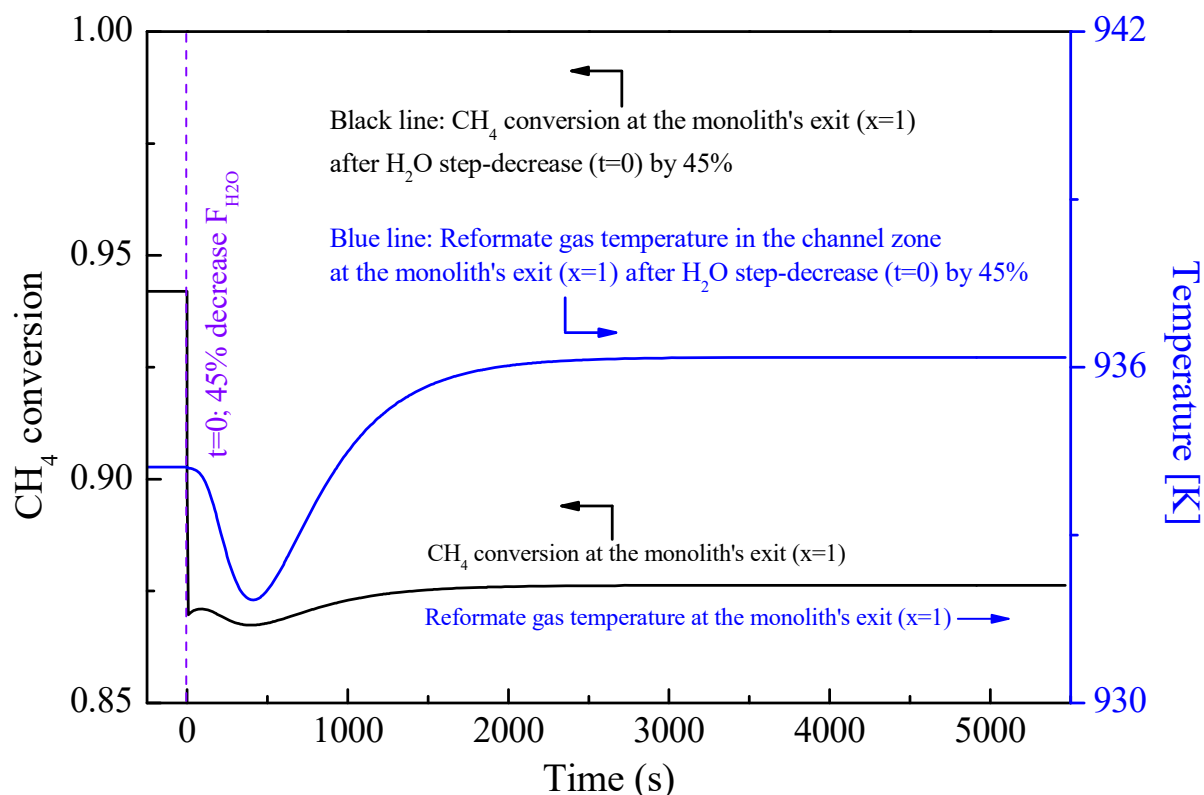

Figure 17: Transient CH₄ conversion and reformate gas temperature profiles in the channel zone (averaged over y) for a step-H₂O decrease (t=0) by 45%.

Figure 19 illustrates the response and the evolution of the flowrates at the channel's exit for the step H_2O-decrease case for 50 s; again, an interpretation of the flowrates' short-term response is attempted according to the analysis of the four-reaction scheme presented in [1].

The decrease of steam is self-evidently caused by the decrease by 45% of its flowrate. The loss of steam temporarily results to CH_4 consumption due to the CH_4-O_2 oxidation reaction; however, in the long-run CH_4 flowrate increases compared with the original (optimal) case because of less-steam-than-needed for the reforming reactions. Lack of steam in combination with the high temperatures facilitates the rWGS reaction leading to CO formation at the expense of CO_2 and H_2. In the long-run this trend remains since temperature remains at these levels.
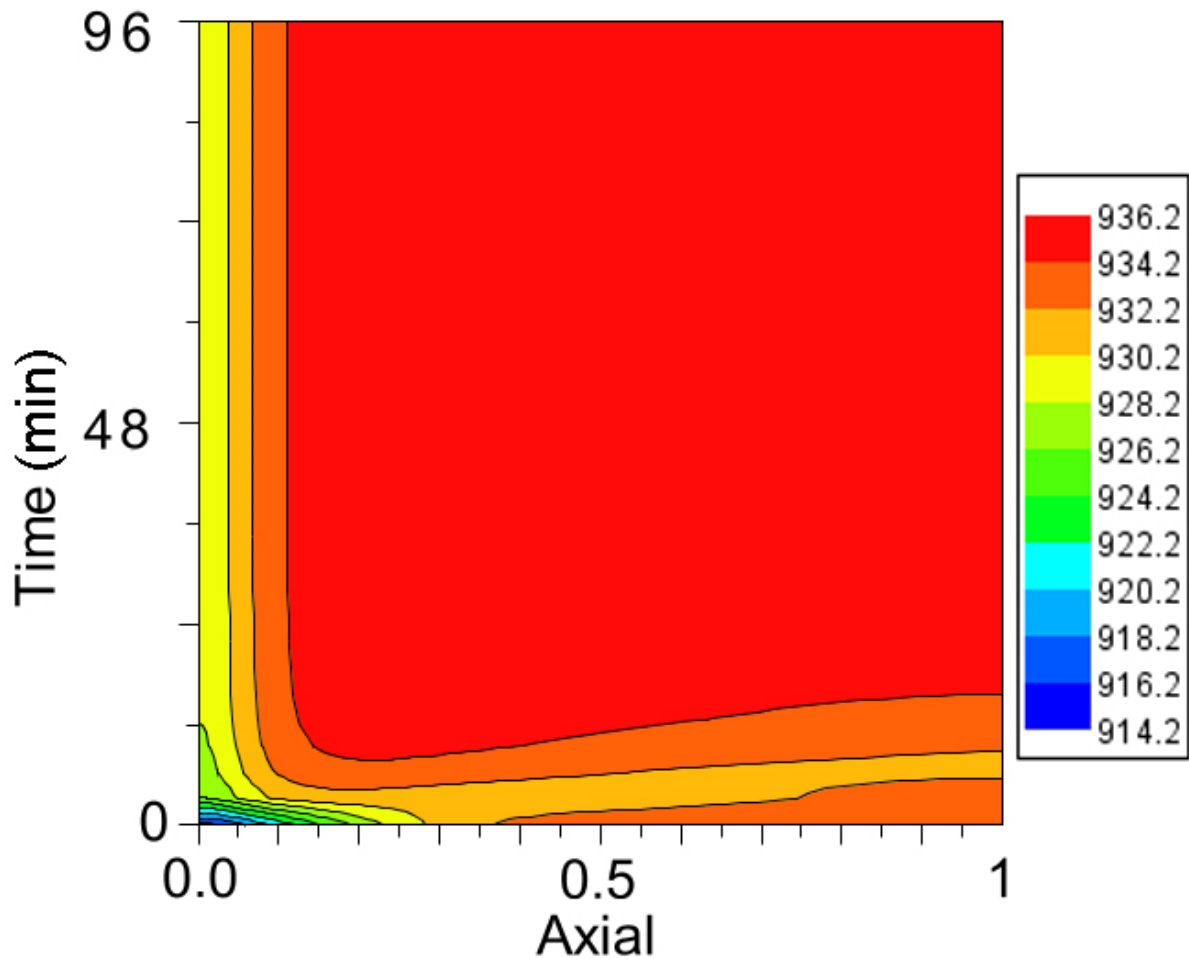
Figure 18: Transient temperature profiles at the washcoat-strut interface for a step-H₂O decrease (t=0) to 45%.

3.6 Catalyst deactivation

A case of major importance is catalyst deactivation over time. The rate of deactivation (function of deactivation with respect to time) can be established by comparing with the long-term data derived during pilot-scale data, or by a dedicated lab-scale experimental campaign. To this end, as the deactivation extent vs. time is largely unknown, this study investigates the steady-state effect of deactivation by assuming a deactivation factor multiplied with the reaction rates of the autothermal reforming scheme (the reader is referenced to [1] for the reaction rates). The profiles presented in Figure 20 resemble a case with all catalytic sites (i.e. the whole length of the catalyst) equally deactivated and are valid for each deactivation factor over the long-run (under steady-state conditions) as long as deactivation of the catalyst does not further worsen over the transition period to reach a new steady-state, that is, roughly not before 80-90 min of operation (see sections 3.2 through 3.5).

Figure 20 depicts the CH_4 conversion over the channel length under steady-state conditions for three deactivation factors and comparison with a fresh catalyst (no deactivation – see section 3.2) – note that an *x %* deactivation denotes that the reaction rates are multiplied with (100-x)/100. As the performance of the catalyst deteriorates, the same conversions as that of the no-deactivation-case are reached at extended distance, e.g. for

the fresh catalyst a conversion of 0.92 is reached at $\overset{\$}{x}$=0.21, for 10% deactivation at $\overset{\$}{x}$=0.235, for 50%

deactivation at $\overset{\$}{x}$=0.37, while for 90% deactivation the conversion of 0.92 cannot occur within the length of the chosen monolith, so that the replacement of the catalyst is mandatory.
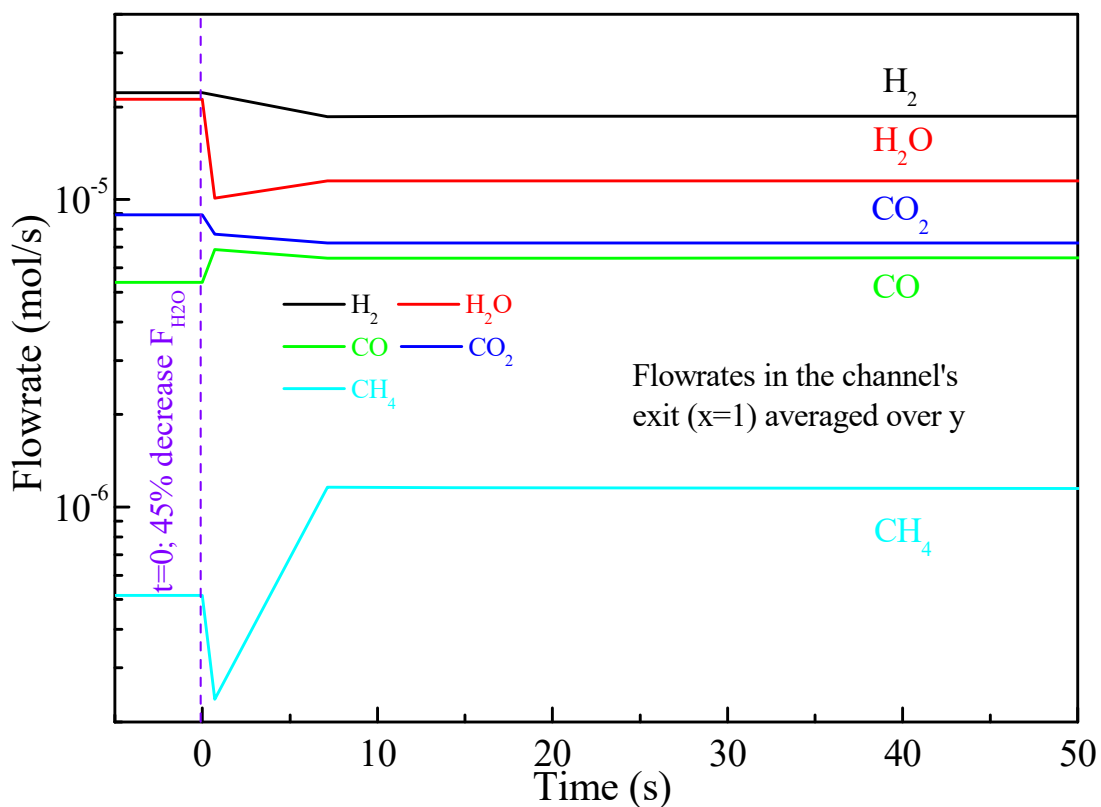
Figure 19: Transient molar fraction profiles in the channel zone (averaged over y) for a step-H₂O decrease (t=0) by 45% for the first 50s after the step-change.
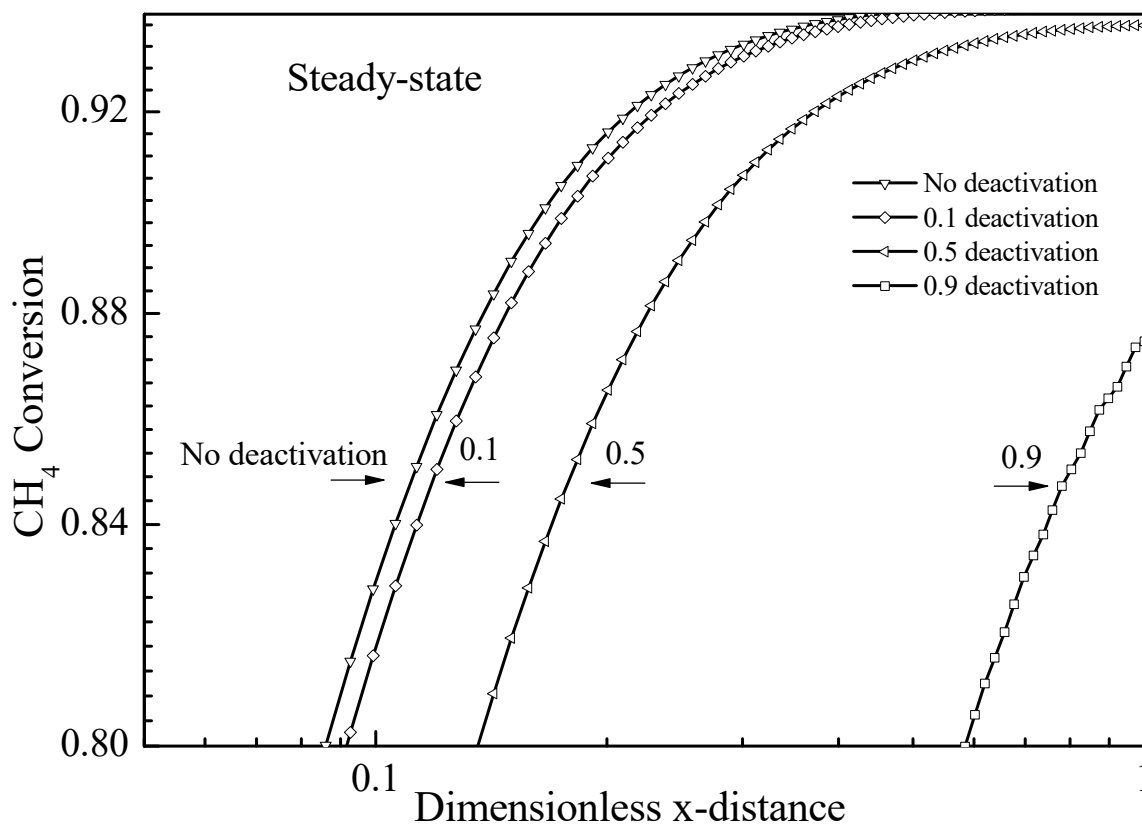

Figure 20: Steady-state CH₄ conversion profiles in the channel zone (averaged over y) for different catalyst deactivation values along

$$\hat{x}.$$

4.   Conclusions

In the previous lines an extended dynamic simulation model is studied for the schedule sequence of the monolith start-up procedure including the system response when a disturbance is imposed after the monolith-reforming system has reached steady-state conditions. In this report the optimization procedure has been conducted once again to account for the updated data for the washcoat-catalyst zone according to correspondence and cooperation with the partners Johnson Matthey and Engicer. The dynamic simulation shows that for both the cold and the hot start-up procedure (excluding catalyst deactivation) the time required reaches 5 h of continuous operation.

It is shown that in the cold start-up operation the monolith steady-state temperature equal to the air temperature (1045.4 K with a deviation of $\leq$0.1%) is reached after 4.35 h. Close to $\hat{x}=0$ the outer strut's wall temperature reaches faster air's temperature and eloquently steady-state temperature (1045.4 K), rather than the upper point at $\hat{x}=1$. Temperature snapshots with respect to $\hat{x}$ and $\hat{y}$ of the gas temperature in the channel zone also reveal that there is variation with respect to $\hat{y}$ especially in the first time periods, whereas $\hat{y}$-gradients flatten at later times and for $\hat{x}\geq$0.1.

When the monolith has reached the desired reforming temperature, the biogas mixture along with O_2 enter the monolith reactor at 1045.4 K, switching from an air mixture to the biogas-O_2 mixture at the same temperature T_0=1045.4. Due to the fact that solid materials are already at the required temperature, catalytic reactions at the washcoat initiate rather instantly, and methane conversion exceeds 94.2% under steady-state conditions, which are reached after 78 min. The system response in a hot start-up case is much faster than the cold start-up case because of the higher heat inertia terms in the latter case that have to be overpassed.

The third and final step of the dynamic simulation cases involve operation under disturbances, that is, after the reforming process has reached steady-state conditions the system is perturbed from steady-state by introducing changes in the assigned values of temperature and feed composition. The first disturbance from the (previous) steady state concerns the decrease of the feed temperature by 50 K. Two cases are considered; first, a step decrease (at t=0$^+$) of 50 K is imposed. The second case assumes that the furnace heating the feed gas has been imposed a temperature ramp decrease of 15 K/min ending to 50 K decrease (that is, ending after 200 s having a value of 945.4 K). It can be concluded that for smaller temperature ramp values the temperature decrease in the wall, and consequently in the washcoat, is not so severe, since for the step-change case the minimum value is 870.6 K, while for the temperature-ramp case the minimum is 882.1 K. Both cases reach the new steady-state profile after 91.4 min.

It is shown that for both cases there is a time lag for the profiles to get the information at the exit of the channel compared to the inlet, since the profiles are steeper close to the inlet and smoother near the exit. Comparing the two cases the temperature-ramp case is smoother than the step-change case because of the higher minimum temperatures in the former case. Both cases exhibit the same final CH_4 conversion reaching 90.6 % after 91.4 min: the new steady-state conversion is significantly lower than that of the optimal case because of the decrease of the inlet temperature by 50 K.

In a new disturbance-case, instead of temperature changes the composition of the biogas-O_2 mixture is altered. In this case, a step-decrease of the O_2 supply by 50% is imposed at t=0$^+$ (T_0 remains at 1045.4 K). The inadequacy of the O_2 amount to sustain the autothermal mode is more pronounced in the O_2-decrease case leading to a drop of the final steady-state CH_4 conversion to 67.6 % after 90 min of operation. However, the temperature response does not follow the response of the conversion, but it has a delay; in this case the eventual temperature decrease to appear in a short course of time would be an indirect result of the smaller oxidation rate of CH_4, and not by any direct temperature decrease of the feed mixture as in the previous case. Still, this temperature drop does not entail that any carbon may be produced: even if no O_2 is present thermodynamic modelling analysis reveals that temperature has to drop below 500 K for potential carbon formation conditions.

The last disturbance-case involves altering the composition of the steam supply (step-decrease) by 45% at t=0$^+$ (T_0 remains at 1045.4 K). The sudden drop of steam entering the monolith causes a step change in the CH_4 conversion at the channel's exit to less than 90%, a value that is roughly maintained during the autothermal reforming mode, ending to 87.6% after 90 min. The temperature response does not follow the conversion's response, but it has a delay, as in the case of the oxygen-step change. Since steam comprises the major fraction

of the feed stream, its flowrate's sudden drop may cause a slight cooling of the solid material and subsequently of the gas temperature as well.

Catalyst deactivation over time has been also studied by assuming a deactivation factor multiplied with the reaction rates of the autothermal reforming scheme. It is shown that as the performance of the catalyst deteriorates, the same conversions as that of the no-deactivation-case are reached at extended distances, e.g. for the fresh catalyst a conversion of 0.92 is reached at $\overset{\$}{x}$=0.21, for 50% deactivation at $\overset{\$}{x}$=0.37, while for 90% deactivation the conversion of 0.92 cannot occur within the length of the chosen monolith, so that the replacement of the catalyst is mandatory.

5.   References

1.   Pantoleontos, G., Vlachos, N., Skevis, G., Lorentzou, S., D2.4: Optimal heat profiles to facilitate the biogas reforming, FCH-02-2-2016. Development of compact reformers for distributed bio-hydrogen production.
2.   Pantoleontos, G., Kikkinides, E.S., Georgiadis, M.C., A heterogeneous dynamic model for the simulation and optimisation of the steam methane reforming reactor, Int. J. Hydrogen Energ. 37 (2012) 16346-16358.
3.   Adams II, T.A., Barton, P.I., A dynamic two-dimensional heterogeneous model for water gas shift reactors, Int. J. Hydrogen Energ. 34 (2009) 887-8891.
4.   Ipsakis, D., Voutetakis, S., Papadopoulou, S., Seferlis, P., Optimal operability by design in a methanol reforming-PEM fuel cell autonomous power system, Int. J. Hydrogen Energ. 37 (2012) 16697-16710.
5.   Ipsakis, D., Ouzounidou, M., Papadopoulou, S., Seferlis, P., Voutetakis, S., Dynamic modeling and control analysis of a methanol autothermal reforming and PEM fuel cell power system, Appl. Energ. 208 (2017) 703-718.
6.   Aslanjan, J., Klauer, C., Perlman, C., Günther, V., Mauss, F., Simulation of a three-way catalyst using transient single and multi-channel models, SAE Tech. Papers (2017) 2017-01-0966.
7.   Jahn, R., Šnita, D., Kubíček, M., Marek, M., 3-D modeling of monolith reactors, Catal. Today 38 (1997) 39-46.
8.   Ghouse, J.H., Adams II, T.A., A multi-scale dynamic two-dimensional heterogeneous model for catalytic steam methane reforming reactors, Int. J. Hydrogen Energ. 38 (2013) 9984-9999.
9.   Hayes, R.E., Kolaczkowski, S.T., Thomas, W.J., Finite-element model for a catalytic monolith reactor, Comput. Chem. Eng. 16 (1992) 645-657.
10.   Hayes, R.E., Kolaczkowski, S.T., Thomas, W.J., Titiloye, J., Transient experiments and modeling of the catalytic combustion of methane in a monolith reactor, Ind. Eng. Chem. Res. 35 (1996) 406-414.
11.   Psyllos, A., Philippopoulos, C., Modelling of monolithic converters with axial catalyst distribution, Appl. Math. Model. 17 (1993) 459-467.
12.   Hoang, D.L., Chan, S.H., Modeling of a catalytic autothermal methane reformer for fuel cell applications, Appl. Catal. A 268 (2004) 207-216.
13.   Chan, S.H., Hoang, D.L., Ding, O.L., Transient performance of an autothermal reformer – a 2-D modeling approach, Int. J. Heat Mass Tran. 48 (2005) 4205-4214.
14.   Baldea, M., Daoutidis, P., Dynamics and control of autothermal reactors for the production of hydrogen, Chem. Eng. Sci. 62 (2007) 3218-3230.
15.   Seepersad, D., Ghouse, J.H., Adams II, T.A., Dynamic simulation and control of an integrated gasifier/reformer system. Part I: Agile case design and control, Chem. Eng. Res. Des. 100 (2015) 481-496.
16.   Seepersad, D., Ghouse, J.H., Adams II, T.A., Dynamic simulation and control of an integrated gasifier/reformer system. Part II: Discrete and model predictive control, Chem. Eng. Res. Des. 100 (2015) 497-508.
17.   Guojiang, W., Song, T., CFD simulation of the effect of upstream flow distribution on the light-off performance of a catalytic converter, Energ. Convers. Manage. 46 (2005) 2010-2031.
18.   Karagiannidis, S., Mantzaras, J., Numerical investigation on the start-up of methane-fueled catalytic microreactors, Combust. Flame 157 (2010) 1400-1413.

19. Oh, S.H., Cavendish, J.C., Design aspects of poison-resistant automobile monolithic catalysts, Ind. Eng. Chem. Prod. Res. Dev. 22 (1983) 509-518.
20. Zygourakis, K., Transient operation of monolith catalytic converters: a two-dimensional reactor model and the effects of radially nonuniform flow distributions, Chem. Eng. Sci. 44 (1989) 2075-2086.
21. Wanker, R., Raupenstrauch, H., Staudinger, G., A fully distributed model for the simulation of a catalytic combustor, Chem. Eng. Sci. 55 (2000) 4709-4718.
22. NIST Chemistry WebBook, SRD 69, aluminium oxide; silicon carbide.